BULLETIN OF THE POLISH ACADEMY OF SCIENCES
TECHNICAL SCIENCES, Vol. 72(4), 2024, Article number: e149819
DOI: 10.24425/bpasts.2024.149819

Occlusion-aware collision avoidance trajectory planning with potential collision risk assessment for autonomous vehicle

Yubin QIAN[1], Chengzhi DENG[1], Jiejie XU[1], Xianguo QU[2*], and Zhenyu SONG[1]

[1] School of Mechanical and Automotive Engineering, Shanghai University of Engineering Science, Shanghai, China
[2] Defective Product Administrative Center, State Administration for Market Regulation, Beijing, China

Abstract. Motion planning for autonomous vehicles relies heavily on perception and prediction results to find a safe, collision-free local trajectory that adheres to traffic rules. However, vehicle perception is frequently limited by occlusion, and the generation of safe local trajectories with restricted perception poses a significant challenge in the field of motion planning. This paper introduces a collision avoidance trajectory planning algorithm that considers potential collision risks, within a hierarchical framework of sampling and optimization. The primary objective of this work is to generate trajectories that are safer and align better with human driver behavior while considering potential collision risks in occluded regions. Specifically, in occlusion scenarios, the state space is discretized, and a dynamic programming algorithm is used for a sampling-based search to obtain initial trajectories. Additionally, the concept of a driving risk field is introduced to describe potential collision risk elements within the human-vehicle-road environment. By drawing inspiration from graph search algorithms, potential collision risk areas are accurately described, and a cost function is proposed for evaluating potential risks in occluded regions. Drivers typically exhibit conservative and cautious driving behavior when navigating through occluded regions. The proposed algorithm not only prioritizes driving safety but also considers driving efficiency, thereby reducing the vehicle's conservativeness when passing through occlusions. The research results demonstrate that the ego vehicle can actively avoid blind spots and tends to move away from occluded regions, aligning more closely with human driver behavior.

Keywords: occlusion scenarios; active collision; risk assessment; trajectory planning.

1. INTRODUCTION

With the rapid advancement of sensor technologies, such as cameras, millimeter-wave radars and LIDAR, they have found extensive applications in autonomous vehicles and mobile robots. Their primary function is to perceive the surrounding environment and provide guidance for decision-making and planning [1]. The results obtained from perception and prediction play a crucial role in analyzing the interaction behavior between the ego vehicle and other vehicles, and in enhancing the safety of motion planning. However, perceptual occlusion problems are prevalent in structured driving scenarios (as illustrated by the occlusion phenomenon in Fig. 1). These problems result in limited perceptual capacity and introduce uncertainty into motion planning [2]. To mitigate uncertainty and enhance driving safety for autonomous vehicles, it is essential to consider potential risks beyond the field of view in the critical aspect of motion planning.

Currently, trajectory planning for autonomous vehicles is rooted in mobile robot path-planning technology [3]. To meet the requirements of road network structures and traffic rule constraints, a wide range of autonomous navigation technologies have been extensively applied to the field of autonomous driving, accompanied by corresponding improvements [4]. According to the implementation of planning techniques in autonomous driving, planning methods can be roughly classified into five categories: potential field methods, interpolation methods, graphical search methods, sampling methods and numerical optimization methods [5].

Potential field-based planning methods involve introducing the concept of potential fields, where the vehicle's motion is abstracted as a vector field movement. Attractive and repulsive fields are assigned to the vehicle's safety zone and obstacles, respectively. The vehicle's future trajectory is then planned by calculating the resultant force field acting on the vehicle [6].

However, this method relies heavily on accurate modeling of the surrounding environment and is prone to getting trapped in local minima [7]. Interpolation-based planning algorithms generate smooth trajectories by interpolating intermediate nodes between known starting and ending points. This allows the vehicle to reach the endpoint with the desired speed and position. However, this method requires an appropriate interpolation density. A density that is too low affects accuracy, leading to local errors, while a density that is too high affects real-time computation [8]. Graphical search-based planning algorithms primarily involve grid or mesh representations of the environment's state space. They describe the position of objects based on the grid

*e-mail: quxg@dpac.org.cn

Manuscript submitted 2023-06-12, revised 2023-12-28, initially accepted for publication 2024-02-25, published in July 2024.

Fig. 1. Illustration of a hazardous driving scenario with potential collision risks [6]. (The photo, captured by a car's onboard camera, depicts the sudden appearance of a vulnerable road user (VRU) from the left perceptual occluded area. In the subsequent frame, an unavoidable collision occurs between the car and the VRU)

cells they occupy and derive a movement path by traversing the state space. Such algorithms are widely utilized in the field of robot motion planning [9]. However, the paths planned by these algorithms are not necessarily optimal and do not consider road geometry constraints, resulting in poor trajectory smoothing.

At present, methods capable of performing motion planning tasks for autonomous vehicles on structured roads can be categorized into two main types: sampling-based methods and numerical optimization-based methods [10].

With sampling-based methods, it is possible to intuitively express abstract and complex spaces and find global optimal solutions in discrete and complex road environments. On the other hand, numerical optimization-based methods utilize precise modeling principles to converge rapidly towards minimum values and find local optimal solutions [11]. Therefore, most advanced motion planning solutions for autonomous vehicles combine the advantages of the aforementioned approaches, establishing a hierarchical framework that involves sampling first and then optimizing.

In the field of motion planning research for mobile robots, the dominant challenge currently arises from the uncertainty and unknown introduced by the limited field of view. The primary approach to addressing this issue is to reduce the area of unknown regions through various measures, thereby improving the perceptual limits. For instance, slowing down the robot's speed, adjusting its trajectory, and selecting higher-curvature trajectories when approaching occluded areas [12]. These methods emphasize the visibility of trajectories by introducing trajectory constraints, allowing the robot to fully perceive the previously occluded areas before reaching them.

To solve the problem of limited perceptions, the literature [13] describes the perception objective formulation in terms of the objective function of the optimal control problem, and it enhances the visibility input based on the MPC method, thereby improving the perception capability of the occluded area. Passage safety is improved by predicting current and future movement occupancy. Some scholars propose a path-planning algorithm that considers limited visibility [14], using a sampling-first optimization framework. In the sampling-based coarse trajectory planning layer, an A* searcher with improved heuristic functions is introduced to select 3D trajectories with a better field of views (FOVs), after which a refined trajectory is derived as the initial range of values for the optimization layer while addressing the issue of restricted sensor perception [15]. Some studies consider hidden vehicles behind obstructing obstacles and assume that these vehicles adhere to traffic rules. They investigate the potential collision states and the set of reachable trajectories that can be avoided. Related research is also found in [16].

Nevertheless, in structured road environments, the issue of sensor occlusion for vehicles is more severe than the limited field of view problem faced by mobile robots [17]. The occluded objects within road blind spots exhibit dynamic complexity and motion uncertainty, such as the challenge of avoiding collisions with vulnerable road users (VRUs) present in occluded areas. Therefore, a sole emphasis on trajectory visibility or the complete elimination of occluded areas is limited for autonomous driving motion planning [18]. We also need to consider the collision risk in areas with an occluded field of view.

This paper, grounded in the fundamental nature of collision risk, defines "collision risk" as the amalgamation of collision probability and collision severity [19]. The term "collision risk" is conventionally associated with the degree of harm inflicted upon drivers, passengers and other participants in traffic scenarios, as collisions represent the direct causative factor of injury to these entities. Collision probability is employed to delineate the likelihood of a vehicle engaging in a collision with surrounding traffic participants or obstacles during its course of operation. Meanwhile, collision severity serves as a metric to quantify the extent of harm inflicted upon drivers, passengers and other traffic participants as a consequence of collisions.

The current collision risk assessment methods are divided into deterministic assessment methods, probabilistic assessment methods, reachable set assessment methods and potential field theory-based assessment methods [20]. Among them, the potential field theory-based assessment methods can simultaneously consider multiple scenario elements for risk assessment. Their assessment results can characterize the risk of the main vehicle more comprehensively, and also reflect future risks [21]. Wang, Fu *et al.* propose an algorithm for active sensing, which explores

information about the surrounding environment through a cycle between sensing and trajectory generation to reduce the risk of uncertainty in the environment [22]. Furthermore, Wang *et al*. [23] incorporated visibility prediction into trajectory planning and proposed a prediction-based visibility risk metric that penalizes trajectories with high speed and low visibility.

Recent related research has also explored the integration of motion prediction, collision probability prediction, and collision risk assessment into the longitudinal velocity planning framework, enabling autonomous vehicles to safely navigate through occluded areas. However, these methods only involve longitudinal velocity control and do not address lateral motion planning. As a result, vehicles tend to be more cautious and conservative when passing through occluded areas [24].

To address this issue, this study focuses on generating safer trajectories on perception-limited structured roads. Firstly, a hierarchical motion planning framework, employing a sampling-based approach followed by optimization, is proposed. This framework incorporates a risk assessment method based on potential fields theory to mitigate uncertainties and unknowns caused by occlusions. Secondly, inspired by graph-search algorithms, a potential collision risk evaluation cost function is introduced for occluded regions. Finally, a quadratic programming method is utilized to derive precise and smooth trajectories, enabling the vehicle to safely navigate through obstructed areas without collisions. The framework structure of this paper is shown in Fig. 2. The remaining work in this paper also includes the aspects listed below.

Section 2 describes the trajectory planning problem addressed in this study. Sections 3 and 4 introduce a collision avoidance trajectory planning algorithm that considers potential collision risks in occlusion scenarios. Section 5 presents simulation results and discussions. Section 6 summarizes the contributions and limitations of this study, and discusses future research directions and challenges.

2. PROBLEM STATEMENT

The main objective of this study is to address the motion planning problem for autonomous vehicles in structured road environments with limited perception capabilities, as illustrated in Fig. 3. To tackle this challenge, the paper proposes a method that aims to find a safe and collision-free trajectory for autonomous vehicles, satisfying both dynamic constraints and passenger comfort, by evaluating the potential collision risks in occluded areas. This approach also aims to avoid blind spots and minimize the possibility of potential collisions.

In this paper, we represent the vehicle's state curve at a given moment t as $k(t)$ and the control variable as $u(t)$. The road space for local trajectory planning is defined as S, where S_{obs} represents the region occupied by static obstacles. The vehicle's motion trajectory must not overlap with the region occupied by obstacles, and we define the feasible motion region as $S_{\text{free}} = S/S_{\text{obs}}$.

When the vehicle transitions from one state k_i to another determined state k_{i+1}, a set of control variables $u(t)$ needs to be calculated using the state transition equation while satisfying various hard constraints and soft constraint conditions. Therefore, this paper describes the motion planning problem as an optimal control problem (OCP).

$$\begin{aligned} &\min J\left[k(t), u(t)\right], \\ &\text{s.t. } \Phi\left[k(t), u(t)\right] = 0, \quad t \in [0, T], \\ &k(0) = k_{\text{init}}, \quad u(0) = u_{\text{init}}, \\ &G_{\text{end}}\left[k(T), u(T)\right] \le 0, \\ &G_{\text{collision}}\left[k(t), u(t)\right] \le 0, \quad t \in [0, T], \end{aligned} \tag{1}$$

where T is defined as the required unit cycle time for local trajectory planning. J represents the cost function, and $\Phi = 0$ denotes the dynamic hard constraint conditions that must be satisfied throughout the moving process. k_{init} represents the initial value

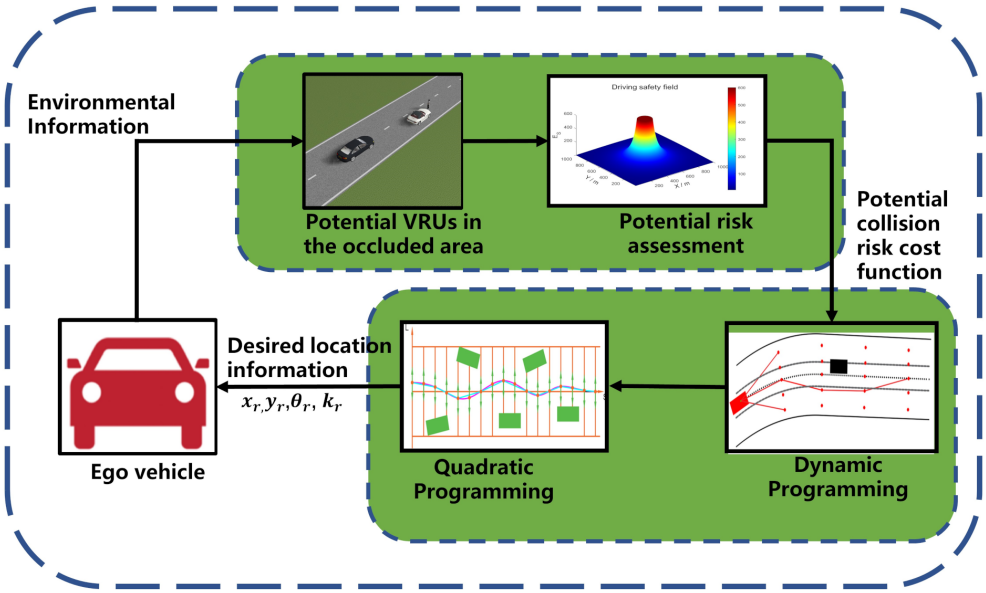

Fig. 2. Schematic diagram of the overall framework

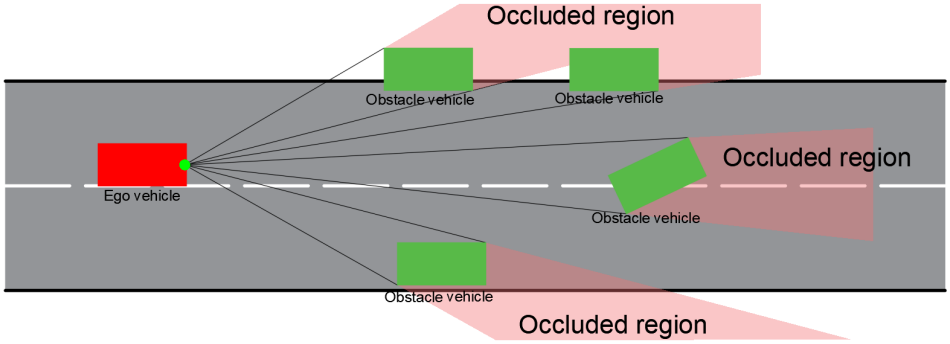

Fig. 3. Schematic diagram of potential collision risk zones in structured road environments

of $k(t)$ at $t = 0$, while u_{init} represents the initial value of $u(t)$ at $t = 0$. $G_{\text{end}} \leq 0$ represents the inequality constraint conditions that the vehicle needs to satisfy upon reaching the destination, such as velocity and pose. $G_{\text{collision}} \leq 0$ represents the collision avoidance constraint conditions that must be satisfied throughout the computation process.

In structured road environments, the typical blind spot scenarios are primarily caused by static obstacles and parked vehicles on both sides of the road, as shown in Fig.]3. Therefore, when conducting motion planning under limited perception capabilities, it is necessary to sample along the perceived boundaries of the road and avoid sampling in prohibited hazardous areas.

Based on the rough trajectory obtained through the sampling method, this paper employs a numerical optimization method to solve the equation for a set of control variables, denoted as $u(t)$, and to satisfy various constraints including dynamic constraints, road geometry characteristics, potential collision risks, and others. By solving the equation for the minimum convergence point of the cost function, the control variables $u(t)$ are obtained, thereby optimizing the desired driving trajectory. The overall framework of the paper is illustrated in Fig. 2.

In addition to considering stationary obstacles, this paper also takes into account the occluded areas formed by these obstacles, where vulnerable road users (VRUs) such as pedestrians, cyclists and motorcyclists may suddenly appear. Therefore, when conducting motion planning with limited sensor perception capabilities, special attention needs to be given to these occluded areas that pose potential collision risks.

To comprehensively consider the coupled effects of various factors such as human-vehicle-road interactions on motion planning, we introduce the concept of the "driving risk field" to quantitatively analyze the potential collision risks of elements in the driving environment. The driving risk field theory can be understood as a force field that describes the risks encountered by a driving vehicle, using physical quantities such as field strength, force and potential energy to describe the risks faced by the vehicle. Information such as the position and velocity of obstacles is used to calculate their contributions to this force field. In motion planning, the potential collision risks should be treated as strict constraints to avoid collisions.

By integrating information from static obstacles, potential VRUs and driving safety fields, effective motion planning can be carried out to minimize collision risks when autonomous vehicles are operating with limited perception capabilities. Therefore, this study focuses on generating safer trajectories within occlusion regions that pose potential collision risks. It is worth noting that the occluded areas created by moving obstacles will be taken into account in speed planning for subsequent stages of the work.

3. DYNAMIC PLANNING BASED ON POTENTIAL RISK ASSESSMENT

This section introduces the proposed trajectory planning algorithm. To reduce search complexity and ensure real-time performance, the algorithm is based on the *Frenet* framework, which uses dynamic planning to search for trajectories with optimal sampling resolution. At the sampling-based trajectory planning stage, the potential collision risk in occluded regions is taken into account by introducing the theory of driving risk fields to assess the potential risk associated with the coupled human-vehicle-road factors. The trajectories planned in the sampling phase are referred to as rough trajectories, and they provide explicit guidance for the vehicle to navigate around on the left or right side to avoid collisions with other traffic participants. The main objective of this section is to search for a reference trajectory, which serves as an initial reference value for the numerical optimization solution phase. This is crucial for generating precise trajectories. The section will provide a detailed explanation of how to generate coarse trajectories that satisfy the constraints.

3.1. Generation of a dynamic programming search space

Currently, in consideration of the increased complexity and real-time performance of the trajectory search due to curvature factors in structured roads, the *Frenet* coordinate system is widely adopted for computational convenience. The *Frenet* coordinate system uses the global path as the reference line and transforms the road centerline with varying curvature in the Cartesian coordinate system into a longitudinal guideline in the $S-L$ diagram.

By employing the coordinate transformation between the *Frenet* and Cartesian coordinate systems, the $S-L$ diagram represents the complex geometric relationships between lanes simply and clearly using the lateral offset L based on the longitudinal guideline S, as illustrated in Fig. 4. Thanks to the

computational advantages of the *Frenet* coordinate system, the trajectory search problem is simplified in complex structured roads with varying curvature, providing a clear illustration of the complex motion of vehicles in roads with varying curvature.

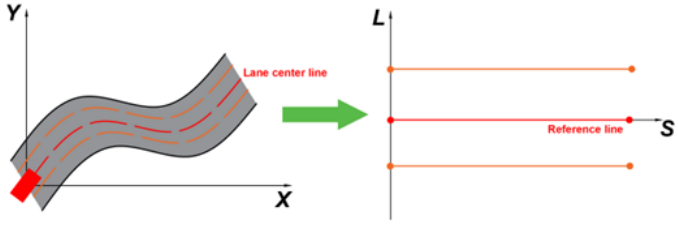

Fig. 4. Schematic diagram of the conversion between the *Frenet* and Cartesian co-ordinate systems

Initially, the range and shape of the search space are determined based on the reference lines. Then, the length of the longitudinal guideline and the range of lateral offset sampling points are defined along the reference lines, discretizing the search space into a series of grids.

The vertices of these grids can be represented by N_{ij}, where i and j denote the row and column numbers of the grid, respectively. The sampling points in the discretized space are generated according to the following rules:

$$S = i \cdot \Delta s, \tag{2}$$

$$L = j \cdot \Delta l. \tag{3}$$

Indices i and j represent the index directions of S and L, within the safety index range, ΔS represents the unit spacing divided in the S index direction, and Δl denotes the lateral offset of the sampled vertex N_{ij} from the reference line. The magnitude of the offset depends on factors such as the vehicle's movement speed, road geometry, lane-changing driving behavior, etc.

The set of sampling points N_{ij} with the same longitudinal distance is defined as a layer, and by combining different $Layer_i$, the search space within a search period T is discretized, as shown in Fig. 5. A coarse trajectory candidate refers to a group of continuous search edges in the discretized search space, which is obtained by dynamically planning to compute sampled points that satisfy various constraints in the next layer.

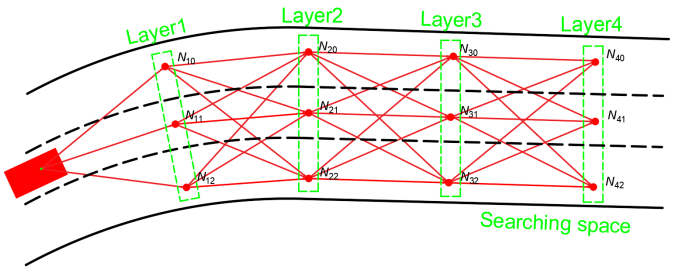

Fig. 5. Searching the space in a Cartesian coordinate system

Similarly, when the ego vehicle is in $Layer_i$, the sampled points in the next $Layer_i$ can also be obtained. By connecting the sampled points in each layer with consecutive edges, a coarse trajectory that satisfies the constraints can be generated, as shown in Fig. 6. The intention of generating a coarse trajectory is to guide the vehicle to travel along the reference line S while avoiding collisions with obstacles. We evaluate the quality of the trajectory candidates by designing a cost function.

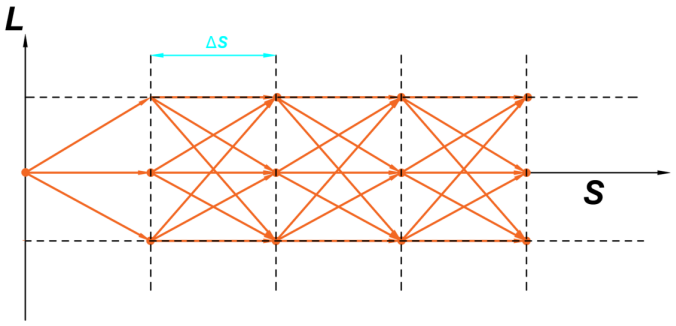

Fig. 6. Search space in the *Frenet* coordinate system

3.2. Cost function based on potential risk assessment

Behavioral trajectory candidates represent the various driving motivations of autonomous vehicles on structured roads and the selection of optimal driving behaviors. In this subsection, behavioral trajectory candidates for autonomous vehicles are evaluated by designing a cost function to select optimal driving behavior. We follow the cost function design guidelines widely used in decision planning algorithms and design a collision avoidance cost function, a driving efficiency cost function and a lane guidance line cost function. And we introduce the theory of driving safety field and propose a cost function for assessing the potential collision risk.

3.2.1. Cost function $J_{\text{potential risk}}$ considers the occluded region with potential collision risk

In this subsection, we will explain how to establish the potential collision risk function $J_{\text{potential risk}}$. The cost function takes into account the possibility of collision risk for vehicles in blind or occluded regions. When a vehicle is driving in an occluded area, there is a high risk of collision with a vulnerable road user (VRU) that suddenly appears from the blind area, as shown in Fig. 7. Therefore, to avoid such situations, it is necessary to impose relevant penalties on the vehicle to ensure its safe passage through the occluded region.

When driving on structured roads, various factors such as driver characteristics, road users and road conditions can affect safety of the vehicle. The interaction between these factors can pose threats to vehicle movement. In this study, based on the theory of driving safety fields, we assess the potential collision risk in the blind zones caused by occlusion factors and the potential sudden appearance of VRUs in structured roads.

Based on the generated search space using dynamic programming, let's assume that the vehicle is located in $Layer_i$ of the spatial state. At this point, we need to evaluate the potential collision risk for the coarse trajectory between the current $Layer_i$ and the adjacent next $Layer_{i+1}$. The spatial position between

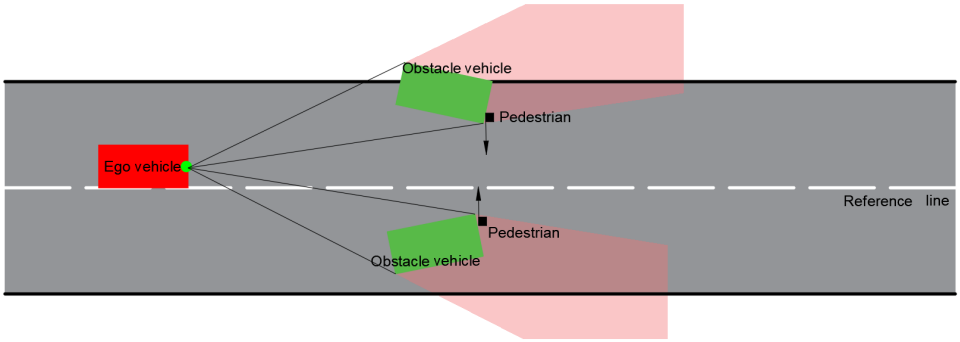

Fig. 7. Schematic representation of a hazardous scenario where a vulnerable road user (VRU) suddenly appears from an occluded region

adjacent layers is determined by the following equation:

$$Layer_{i+1} = Layer_i + \Delta s. \tag{4}$$

Additionally, the mileage of $Layer_i$ can also be calculated in the same way. Therefore, we can estimate the average speed of the vehicle during the transition from $Layer_i$ to $Layer_{i+1}$.

$$v = \Delta s \cdot (N_s - 1)/T, \tag{5}$$

where N_s is the number of layers sampled per sampling period T. Firstly, the time frame in the current $Layer_i$ is defined as T_i, and the time frame in the neighboring $Layer_{i+1}$ is T_{i+1}. Therefore, when the time is between T_i and T_{i+1}, expressed as $t \in [T_i, T_{i+1}]$, we need to assess the potential collision risk for the coarse trajectory between neighboring layers.

Assuming that the vehicle sensor detects obstacles on both sides of the road at time frame T_i, as shown in Fig. 7, we can construct the driving risk potential field, as shown in Fig. 8, based on the driving risk field theory, using obstacles as risk sources according to equation (6), and carry out risk assessment.

$$\begin{aligned} E_s &= E_R + E_V + E_D, \\ E_{R,aj} &= E_{R,aj}\left(M_a, R_a, r_{aj}\right), \\ E_{V,bj} &= E_{V,bj}\left(M_b, R_b, r_{bj}, v_b\right), \\ E_{D,cj} &= E_{V,cj} \cdot DR_c, \end{aligned} \tag{6}$$

where E_S denotes the field strength of the driving safety field, E_R denotes the field strength of the potential energy field, E_V denotes the field strength of the dynamic energy field, and E_D denotes the field strength of the behavioral field, while E_S is the sum of E_R, E_V and E_D.

Among them, $E_{R,aj}$ represents the static obstacle field strength vector, indicating that static obstacle a is located at position (x_a, y_a) and will produce a field strength vector at position (x_j, y_j). M_a represents the virtual mass of static obstacle a, R_a represents the road condition impact factor at location (x_a, y_a), and r_{aj} represents the radius of the field strength interaction range, where $r_{aj} = (x_j - x_a, y_j - y_a)$.

Among them, $E_{V,bj}$ is denoted as the dynamic obstacle field strength vector, indicating that dynamic obstacle b is located at position (x_b, y_b) and will produce a field strength vector at position (x_j, y_j). M_b represents the virtual mass of dynamic obstacle b, R_b represents the road condition impact factor at location (x_a, y_a), and r_{bj} represents the radius of the field strength interaction range, where $r_{bj} = (x_j - x_b, y_j - y_b)$. v_b represents the movement velocity of dynamic obstacle b.

$E_{D,cj}$ represents the behavior field strength formed by dynamic obstacles, indicating the potential danger that vehicles pose to surrounding vehicles. $E_{V,cj}$ represents the dynamic obstacle c located at position (x_c, y_c), and the field strength vector it creates at position (x_j, y_j). DR_c represents the vehicle risk factor.

Similarly, in a structured road, we will have randomly parked vehicles as risk sources. We can then construct a road obstacles risk potential field diagram, as shown in Fig. 9. Through Fig. 9,

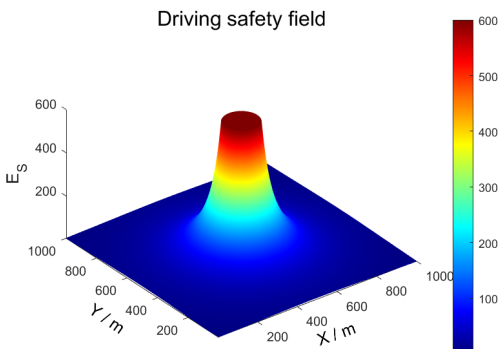

Fig. 8. Driving risk field diagram

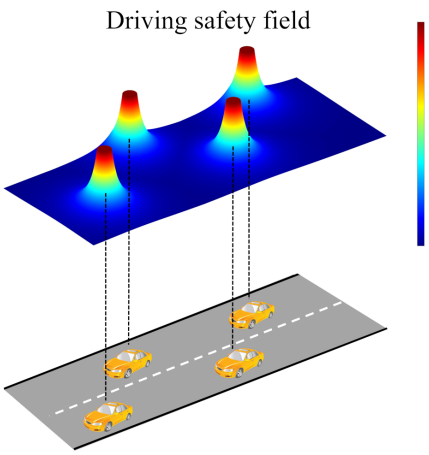

Fig. 9. Risk potential field of road obstacles

we can intuitively discover that the closer the ego vehicle is to the occluded area, the higher its risk value for that area. In order to better quantify and analyze the potential collision risk relationship between the ego vehicle and the potential VRU, we have introduced the idea based on graphical search to rasterize the state space and use the advantage of the grid to accurately describe its spatial location to describe the potential collision risk region.

We project the risk potential field of the occluded region onto the plane of the structured road. We sample the top view along the horizontal and vertical directions, dividing it into $m \cdot k$ grids. This allows us to construct a grid-based representation of the driving risk, known as the risk grid map, to accurately depict the potential collision risk in spatial positions, as illustrated in Fig. 10.

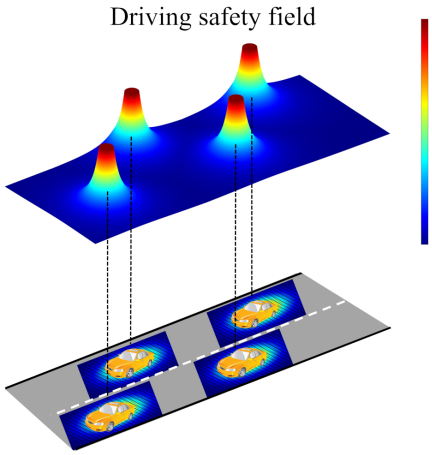

Fig. 10. Risk grid map of the potential driving risk field

We refer to the VRU protection test standards in E-NCAP [25] and define the maximum driving speed of VRU as $v_{\max}$. Then the VRU moving speed interval is expressed as:

$$v \in (0, v_{\max}) .$$

Secondly, for safety reasons, we are considering the worst-case scenario where the vulnerable road user (VRU) unexpectedly emerges from the occluded zone, as depicted in Fig. 7. It is well-known that many traffic accidents occur due to the inattention of the parties involved, leading to failure to perceive potential collision threats. Therefore, we make a reasonable assumption in this study that the VRU is unable to notice the approaching vehicle.

When the sensor detects a VRU suddenly crossing the blind zone at a time frame T_i, the driver usually subconsciously applies emergency braking measures to avoid collision with the VRU. We define the time frame at which the vehicle comes to a stop as T_{end}.

It is worth noting that the focus of this work is on the assessment of potential collision risk for the rough trajectory between time frames T_i and T_{i+1}. If the primary vehicle has stopped before the time frame T_{i+1} and is already at rest before spatial state $Layer_{i+1}$, then there is no need to carry out collision detection for the connected trajectory between the spatial state $Layer_i$ and $Layer_{i+1}$.

It is worth noting that the core of this study is to assess the potential collision risk for the coarse trajectory between time frames T_i and T_{i+1}. If the ego vehicle has already come to a stop before the time frame T_{i+1}, indicating that it is already stationary before spatial state $Layer_{i+1}$, then there is no need to perform collision detection for the connected trajectory between spatial state $Layer_i$ and $Layer_{i+1}$.

However, when $T_{\text{end}} > T_{i+1}$, it indicates that the ego vehicle is still not stopped at spatial state $Layer_{i+1}$, and therefore, the coarse trajectory needs to be selected through potential collision risk assessment. In this case, it is assumed that the VRU moves with a velocity of $(0, v_{\max})$ during the period of $[T, T_{i+1}]$.

For the sake of increased safety, we typically consider the most dangerous scenario, such as when the VRU suddenly emerges from an obstacle and moves toward the center of the road. As shown in Fig. 7, the VRU appears in the sensor's field of view closely adjacent to the obstacle and moves vertically along the obstacle toward the center line of the road.

At this point, based on the risk potential field's grid diagram, we assume that the VRU is located near the occluded area of the field of view. During the current time frame from T_i to T_{i+1}, when the VRU moves at a speed of $v \in (0, v_{\max})$, it occupies a maximum area of N grids. Depending on the level of danger, we define different potential collision risk values for different intervals.

Specifically, we assume that the VRU occupies N_{high} grids in the risk range of 300–450, N_{middle} grids in the range of 150–300, and N_{low} grids in the range of 0–150. Additionally, we have $N = N_{\text{high}} + N_{\text{middle}} + N_{\text{low}}$, where $\text{unit}_{\text{high}}$, $\text{unit}_{\text{middle}}$, and unit_{low} represent the risk costs associated with the occluded area.

$$J_{\text{potential risk}} = unit_{\text{high}} \cdot N_{\text{high}} + unit_{\text{middle}} \cdot N_{\text{middle}} + unit_{\text{low}} \cdot N_{\text{low}} . \tag{7}$$

3.2.2. Collision avoidance cost function J_{obs}

The collision avoidance cost function relies primarily on the distance between the host vehicle and the obstacle to determine whether a collision is likely and whether the corresponding penalty should be applied. Typically, multiple discs are used to cover the area surrounding the vehicle. To reduce computational demand, two discs are used in this paper for covering the vehicle, as shown in Fig. 11. If any of these discs approach or collide with the obstacle, a significant penalty is imposed to the host vehicle. This approach encourages the vehicle to avoid the obstacle and prioritize safety [26].

$$J_{\text{obs}} \begin{cases} 0 & d > d_n \\ J_{\text{nudge}}\,(d - d_c) & d_c \le d \le d_n , \\ J_{\text{collision}} & d < d_c . \end{cases} \tag{8}$$

In the equation above, J_{obs} represents the cost function based on the distance between the ego vehicle and the obstacle, which denotes the distance between them. Specifically, when d is smaller than the set minimum collision distance d_c, the cost

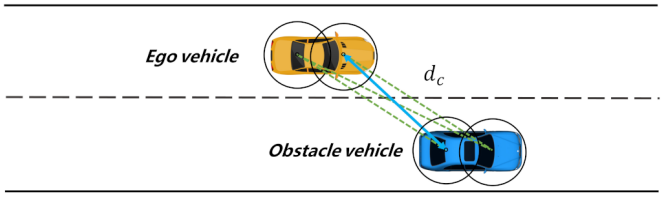

Fig. 11. Environmental constraints keep the host vehicle at a safe distance from the obstacle vehicle

function $J_{\text{collision}}$ will reach a very large value, thus excluding unsafe trajectories. Additionally, d_n is defined as the nudge distance, and we introduce the monotonically decreasing function J_{nudge} to indicate that the collision cost gradually increases as the distance decreases within the range of $d \in [d_c, d_n]$. This effectively guides the self-driving vehicle to avoid collisions with obstacles.

3.2.3. Driving efficiency cost function J_{eff}

The driving efficiency cost function aims to enhance the distance traveled by the vehicle within a unit planning cycle T. By setting a target driving speed, it calculates the difference between the current speed and the target speed to penalize trajectory points with larger differences. This function is designed to improve the vehicle's efficiency when passing through an occluded area. In this context, ds/dt denotes the current speed of the main vehicle, and v_{norm} denotes the target speed.

$$|ds/dt - v_{\text{norm}}|. \tag{9}$$

3.2.4. The cost function for considering the lane reference line J_{ref}

The lane reference line cost function indicates that in the absence of obstacles, the most desirable trajectory of a vehicle on a road is usually the centerline of the lane, where f_{ref} indicates the lane centerline and J_{ref} indicates that a penalty is applied to trajectories with large lateral offsets g_l to encourage vehicles to follow the lane centerline as closely as possible.

$$J_{\text{ref}} = \int (f_{\text{ref}}(s) - g_l(s))^2 \, \mathrm{d}s. \tag{10}$$

Ultimately, we weigh and sum the above cost terms to obtain the total cost function.

$$f_{DP} = \omega_{\text{occ}} J_{\text{potential risk}} + \omega_{\text{obs}} J_{\text{obs}} + \omega_{\text{eff}} J_{\text{eff}} + \omega_{\text{ref}} J_{\text{ref}}. \tag{11}$$

In this section, we introduce the concept of driving risk field at the dynamic planning stage to accurately assess the potential collision risk in the occluded area, and quantify the potential collision risk by establishing a cost function $J_{\text{potential risk}}$. This design ensures the accuracy and validity of potential risk assessment, so that even if the trajectory candidates are all involved in blind collision risk, we can still find the trajectory with the lowest potential collision risk to ensure that the vehicle is safe to drive away from the occluded area. A coarse trajectory generation process is shown in Fig. 12.

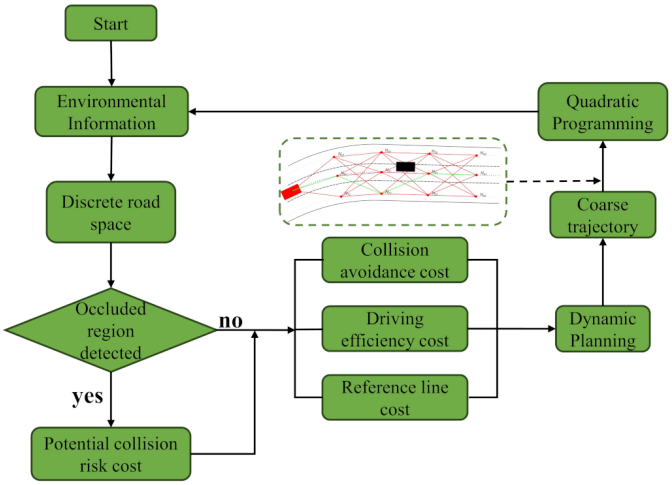

Fig. 12. Coarse trajectory generation process

4. PRECISE TRAJECTORY PLANNING BASED ON QUADRATIC PROGRAMMING

To obtain an accurate trajectory, it is necessary to start with an initial rough trajectory. The derived rough trajectory is represented as $\{(x_i, y_i, t_i) | i = 0, \ldots, N_s\}$. In this step, the rough trajectory obtained from dynamic programming serves as a guiding line and also provides an initial guess for the nudge distance of obstacles. This initial value helps in solving the accurate trajectory. The precise trajectory solving process is shown in Fig. 13.

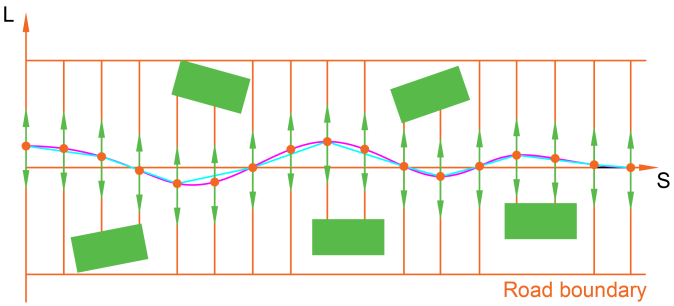

Fig. 13. Trajectory optimization process for quadratic programming. (The obstacles are mapped to the *Frenet* coordinates, and the coarse trajectory serves as the initial value. A smooth reference line S is used as a reference. The spatial coordinates are discretized into a coordinate system with a resolution of Δs, and the upper and lower boundaries of l are defined to solve the road boundaries. The optimization process involves solving the formula for each l_i to optimize the trajectory)

We optimize the solution of the exact trajectory as an optimal control problem (OCP), which involves an objective function and various constraints. Specifically, under different constraints, we employ a quadratic programming-based approach to optimize the objective function of the precise trajectory. Considering the refinement of the coarse trajectory, the objective function is closely related to the costs of trajectory smoothness and adherence to the guideline. To meet requirements such as vehicle kinematic constraints, collision avoidance and trajectory

smoothness, the objective function is defined accordingly.

$$f_{QP} = \sum_{i}^{N_m} \omega_{\text{acc}} J_{\text{acc}} + \omega_{\text{jerk}} J_{\text{jerk}} + \omega_{\text{ref}} J_{\text{ref}} + \omega_{\text{smo}} J_{\text{smooth}}, \quad (12)$$

where N_m represents the total number of trajectory nodes at the optimization stage, penalizing the vehicle's acceleration to ensure smooth driving.

$$J_{\text{acc}} = a_{s,i}^2 + a_{l,i}^2, \quad (13)$$

$$a_{s,i} = \frac{s_{i+1} - 2s_i + s_{i-1}}{\Delta t^2}, \quad (14)$$

$$a_{l,i} = \frac{l_{i+1} - 2l_i + l_{i-1}}{\Delta t^2}, \quad (15)$$

where a_s and a_l denote acceleration along the s and l directions, respectively. This penalty function ensures that the curvature and longitudinal acceleration variations of the precise trajectory are relatively smooth. J_{jerk} is denoted as the rate of change of acceleration and is defined as:

$$J_{\text{jerk}} = j_{s,i}^2 + j_{l,i}^2, \quad (16)$$

$$j_{s,i} = \frac{s_{i+2} - 3s_{i+1} + 3s_i - s_{i-1}}{\Delta t^3}, \quad (17)$$

$$j_{l,i} = \frac{l_{i+2} - 3l_{i+1} + 3l_i - l_{i-1}}{\Delta t^3}. \quad (18)$$

To ensure smooth driving, penalties are applied for sudden changes in acceleration. In particular, $j_{s,i}$ and $j_{l,i}$ represent the jerk along the s and l directions, respectively.

$$J_{\text{smooth}} = k_1 \int (f'(s))^2 \, \mathrm{d}s + k_2 \int (f''(s))^2 \, \mathrm{d}s + k_3 \int (f'''(s))^2 \, \mathrm{d}s. \quad (19)$$

Defining the smoothing cost function as J_{smooth}, the degree of curvature of a trajectory can be reduced by applying a penalty to trajectories with greater curvature, thereby reducing the lateral acceleration of the vehicle during maneuvering and improving maneuvering stability and ride comfort. To be specific, $f'(s)$ is used to represent the heading error between the main vehicle and the trajectory. $f''(s)$ is closely related to the curvature of the trajectory. When the change in curvature is large, a corresponding penalty is imposed by smoothing the $f'''(s)$ term of the derivative of curvature in the cost function to ensure that the change in curvature of the trajectory is small. The lane reference line cost function term J_{ref} in the objective function, referenced to equation (10), is shown.

The smoothing cost function, denoted as J_{smooth}, is defined to reduce the curvature of the trajectory by penalizing trajectories with high curvature. This helps decrease the lateral acceleration of the vehicle during maneuvers, improving both maneuvering stability and ride comfort. Specifically, $f'(s)$ represents the heading error between the main vehicle and the trajectory, while $f''(s)$ is closely related to the curvature of the trajectory. When there is a significant change in curvature, the derivative term $f'''(s)$ in the smoothing cost function applies a corresponding penalty to ensure a smaller change in curvature. The objective function includes the lane reference line cost function term J_{ref}, as shown in equation (10).

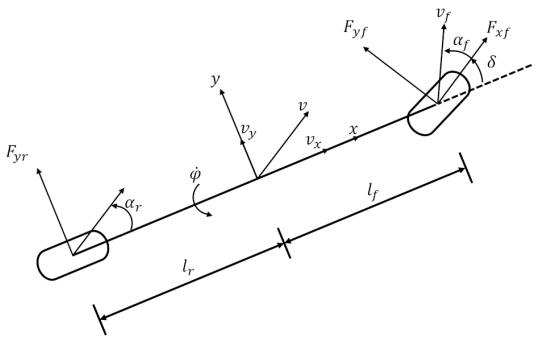

Fig. 14. Vehicle dynamics model

The precise trajectory is not only the convergence point of the objective function's minimum value but it also needs to satisfy vehicle dynamic constraints and surrounding environmental constraints [27]. Considering that the vehicle is a nonlinear system, it is necessary to appropriately simplify the model while reflecting its dynamics characteristics. Therefore, this paper adopts a two-degree-of-freedom vehicle dynamic model, as shown in Fig. 14, with its dynamics equations as follows:

$$\begin{aligned} m\left(\dot{v}_x - v_y\dot{\varphi}\right) &= F_{xf}\cos\delta - F_{yf}\sin\delta, \\ m\left(\dot{v}_y + v_x\dot{\varphi}\right) &= F_{xf}\sin\delta + F_{yf}\cos\delta + F_{yr}, \\ I_z\ddot{\varphi} &= l_f\left(F_{xf}\sin\delta + F_{yf}\cos\delta\right) - l_r F_{yr}, \end{aligned} \quad (20)$$

where m represents the vehicle mass, v_x and $\dot{v_x}$ are the longitudinal velocity and longitudinal acceleration, respectively, v_y and $\dot{v_y}$ are the lateral velocity and lateral acceleration, respectively, $\dot{\varphi}$ and $\ddot{\varphi}$ represent the yaw rate and yaw angular acceleration, F_{xy} is the longitudinal force on the front wheels; F_{yf} and F_{yr} are the lateral forces on the front and rear wheels, δ is the front wheel steering angle; l_f and l_r are the distances from the center of mass to the front and rear axles of the vehicle; l_z is the moment of inertia of the vehicle about the Z-axis; a_f and a_r are the slip angles of the front and rear wheels of the vehicle, x is the coordinate system on the ground, v_f is the front wheel speed, and v is the vehicle speed.

Meanwhile, the precise trajectory is not only the convergence point of the minimum of the objective function, but it also needs to satisfy both the vehicle dynamics constraints and the surrounding environment constraints. The dynamics constraint implies that the acceleration of the precise trajectory should be within the physical limits of the vehicle. Specifically, the sum of the acceleration along the s-direction and the acceleration along the l-direction in the *Frenet* coordinate system should be within the maximum range of the vehicle acceleration.

$$a_{s,i}^2 + a_{l,i}^2 \le a_{\max}^2. \quad (21)$$

Environmental constraints refer to the requirement that the vehicle should avoid collisions with obstacles. Typically, a circular disk model is employed, where both the ego vehicle and obstacles are covered by circular disks [28]. The constraint ensures that the distance between the front and rear axle centroids of both the ego vehicle and the obstacles is greater than the sum of their respective disk radii, as illustrated in Fig. 11. The specific solution process for the quadratic programming problem can be found in reference [29]. We designed a longitudinal double PID controller and a lateral LQR controller according to reference [30], so as to track the precise trajectory solved by quadratic programming.

The process of generating a precise trajectory is shown in Fig. 15.

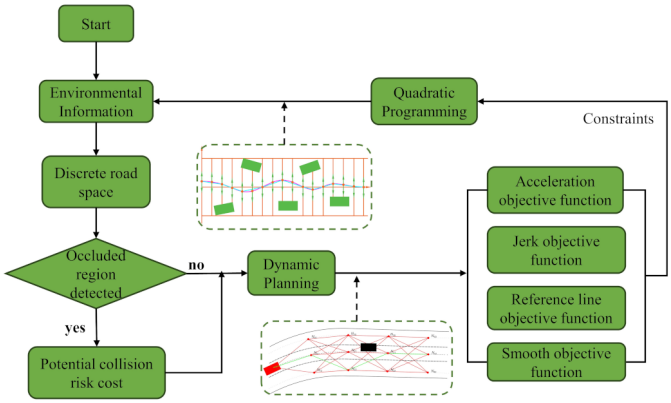

Fig. 15. Precise trajectory generation process

5. SIMULATION CONCLUSIONS AND DISCUSSION

This section reports on simulation results and develops related discussions. The simulations were performed in a joint MATLAB R2020a\PreScan\Carsim simulation using a quadratic programming solver, and executed on a 12th Gen Intel Core i7-12700H CPU with 16.0 GB RAM running on Microsoft Windows 11 running at 2.30 GHz. Key parameters of the simulation were set according to Table 1.

During the simulation verification process, we use gray rectangular modules to represent other vehicles in the surrounding environment. The sizes of these rectangles are based on real vehicle parameters, as shown in Table 1. Furthermore, to validate the effectiveness of the algorithm, we created a simulation scenario as shown in Fig. 16.

Table 1
Simulation parameter setting

Parameters	Value
$v_{\max}$	9.5 m/s
$a_{\max}$	9 m/s^2
m, k	10, 10
k_1, k_2, k_3	60, 40, 20
R_a, R_b, DR_c	5 ,4, 2
Vehicle wheelbase	2.947m
Distance constants d_n, d_c	15, 5
$unit_{\text{high}}$, $unit_{\text{middle}}$, $unit_{\text{low}}$	40, 25, 10
ω_{obs}, ω_{eff}, ω_{ref}	30, 20, 80
ω_{acc}, ω_{jerk}, ω_{smo}	60, 40, 0
Lateral sampling distance Δl	3 m
Longitudinal sampling distance Δs	5 m
Sampling cycle T, Sampling time t	3 s, 0.05 s
Distance from center of mass to the rear axle	1.682 m

Based on the presented simulation results in Fig. 16, it is evident that considering or neglecting potential collision risks results in the generation of significantly different trajectories. Through a comparative analysis of the coarse trajectories, with and without the consideration of potential collision risks, we observe that the introduction of a driving risk field during the coarse trajectory search phase, along with the implementation of a cost function to evaluate potential collision risks in occluded areas, encourages the vehicle to steer clear of such regions before reaching them. This approach greatly expands the sensor's field of view and mitigates the limitations imposed by occluded areas on the vehicle's perception system. Furthermore, these findings align more closely with the driving experience and behavioral patterns of human drivers.

In Fig. 17, we obtained both coarse trajectories and corresponding precise trajectories by considering the potential collision risk. The precise trajectory was derived by formulating the trajectory optimization as an optimal control problem (OCP), with the coarse trajectory serving as the initial solution. By taking into account vehicle dynamics constraints, trajectory smoothness and various other constraints, we were able

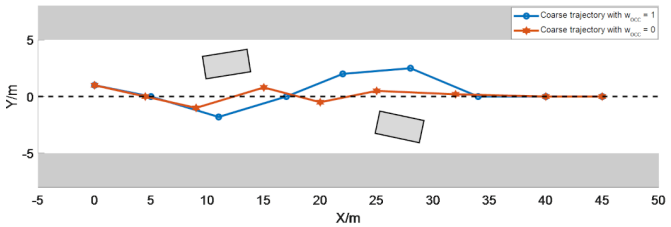

Fig. 16. Avoidance coarse trajectory with and without considering potential collision risks in scenario 1

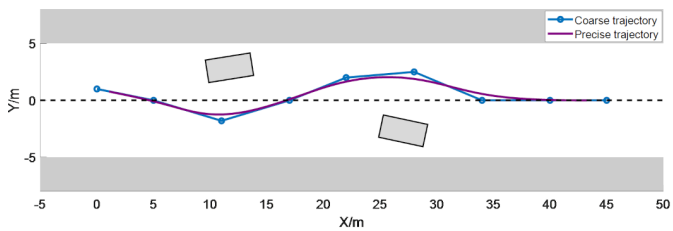

Fig. 17. Coarse and precise trajectory considering potential collision risk in scenario 1

to obtain the final precise trajectory. The optimization process ensured that the resulting trajectory met the requirements of safety, smoothness and adherence to the specified constraints, providing a reliable and optimized path for the vehicle to follow.

The observation indicates that the initial solution serves primarily to provide a reasonable solution space and range for solving the precise trajectory. In the coarse trajectory that considers potential collision risks, the inclusion of risk factors allows for better adherence to safety constraints, resulting in a solution space that aligns more closely with safety requirements for the precise trajectory. Consequently, the ego vehicle possesses the capability to proactively avoid occluded areas, thereby enhancing driving safety.

As shown in Fig. 18, vehicle speed and acceleration are represented on the same axis. Apart from the initial phase where there is significant acceleration fluctuation, acceleration remains stable within a certain range, while vehicle speed increases steadily to the set simulation value. At the same time, Fig. 19 illustrates the yaw rate and sideslip angle of the vehicle. Due to the vehicle's need to actively avoid obstructed areas, the vehicle's motion state parameters exhibit significant fluctuations within a certain range.

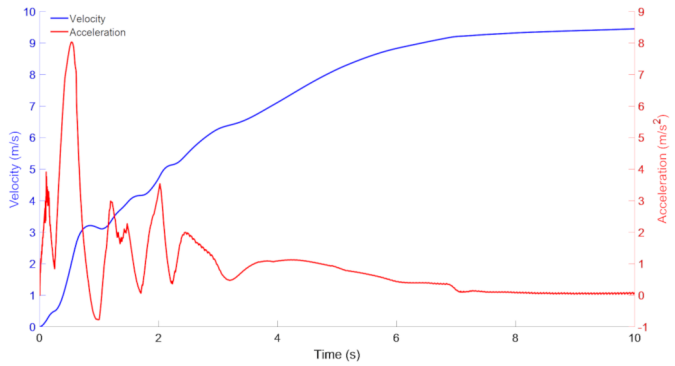

Fig. 18. Velocity profile and acceleration profile in scenario 1

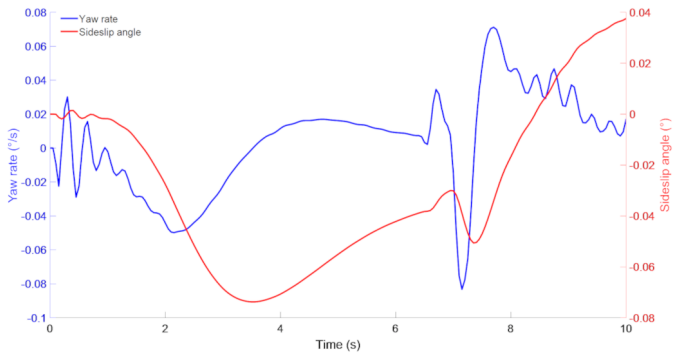

Fig. 19. Yaw rate profile and sideslip angle profile in scenario 1

In the first structured road scenario, we focus primarily on the nudging effect of obstructed areas on lateral motion control of the host vehicle. Additionally, in another scenario, when road conditions do not meet the vehicle's passability requirements, our algorithm computes a relatively safe and conservative trajectory to avoid more severe collision accidents, as shown in Fig. 20.

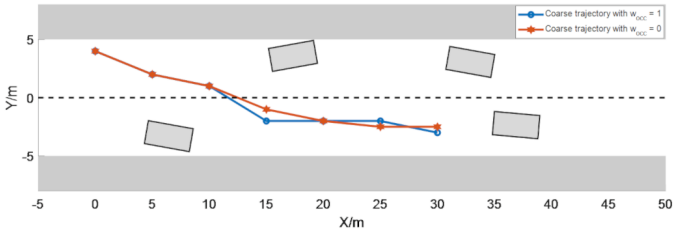

Fig. 20. Avoidance coarse trajectory with and without considering potential collision risks in scenario 2

As shown in Fig. 21, when there are numerous obstacles on the road, and the host vehicle is unable to proceed, to ensure the safety of vehicle operation, our algorithm calculates a more secure and conservative precise trajectory to guide the vehicle to a safe location. At this point, the vehicle's speed and acceleration are represented on the same coordinate axis, as depicted in Fig. 22. The variation in the vehicle speed profile reflects the acceleration phase of the ego vehicle from the beginning of the simulation, followed by gradual deceleration when it becomes impassable, continuing until the end of the simulation. The acceleration curve illustrates that the vehicle undergoes both acceleration and deceleration phases. Additionally, as shown in Fig. 23, the vehicle's yaw rate and sideslip angle reflect significant fluctuations when the vehicle navigates around obstructed areas.

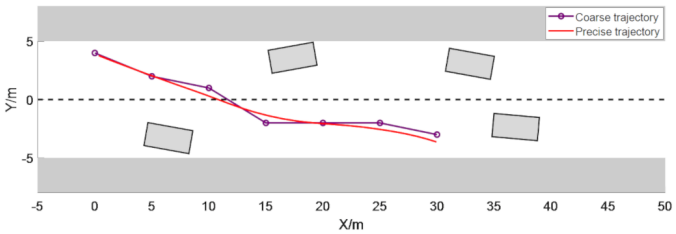

Fig. 21. Coarse and precise trajectory considering potential collision risk in scenario 2

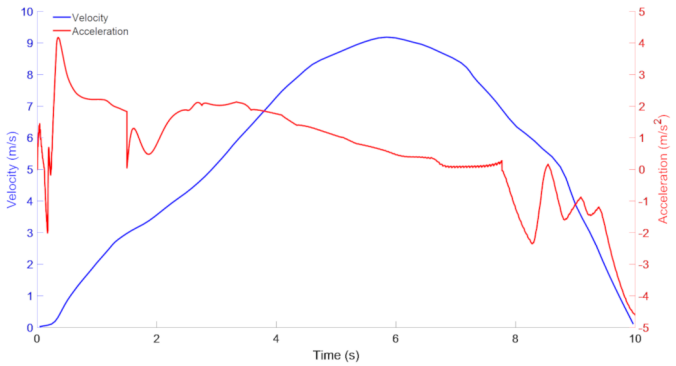

Fig. 22. Velocity profile and acceleration profile in scenario 2

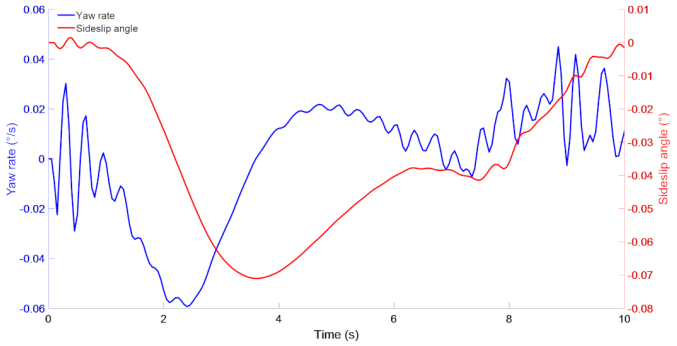

Fig. 23. Yaw rate profile and sideslip angle profile in scenario 2

6. CONCLUSIONS

This paper presents a collision avoidance trajectory planning algorithm for autonomous vehicles in perception-constrained scenarios, taking the potential collision risks into account. The proposed algorithm employs a hierarchical trajectory planning framework, integrating sampling and optimization. During the dynamic planning stage, the concept of driving safety fields is introduced to capture potential collision risk elements within occluded regions.

To accurately represent the spatial distribution of potential collision risks, a driving risk raster map is developed, inspired by graph search techniques. Additionally, to ensure safety, the algorithm considers the most critical driving scenarios near occluded areas and formulates a cost function to assess potential collision risks associated with occlusions.

The precise trajectory solution is obtained by formulating the trajectory planning problem as an optimal control problem (OCP), utilizing quadratic programming. The solution process incorporates various constraints, including vehicle dynamics, trajectory smoothness, safety considerations, etc.

Simulation results demonstrate that the proposed algorithm equips the ego vehicle with the capability to actively avoid occluded areas, mitigating the adverse effects of occlusions and enhancing the vehicle's perception system. These findings align with the empirical knowledge and driving behavior exhibited by human drivers.

REFERENCES

[1] .M. Koschi and M. Althoff, "Set-based Prediction of Traffic Participants Considering Occlusions and Traffic Rules," *IEEE Trans. Intell. Veh.*, vol. 6, no. 2, pp. 249–265, 2021, doi: 10.1109/TIV.2020.3017385.

[2] D. González, J. Pérez, V. Milanés, and F. Nashashibi, "A Review of Motion Planning Techniques for Automated Vehicles," *IEEE Trans. Intell. Transp. Syst.,* vol. 17, no. 4, pp. 1135–1145, 2016, doi: 10.1109/TITS.2015.2498841.

[3] L. Claussmann, M. Revilloud, D. Gruyer, and S. Glaser, "A Review of Motion Planning for Highway Autonomous Driving," *IEEE Trans. Intell. Transp. Syst.,* vol. 21, no. 5, pp. 1826–1848, May 2020, doi: 10.1109/TITS.2019.2913998.

[4] M. Elbanhawi and M. Simic, "Sampling-Based Robot Motion Planning: A Review," *IEEE Access,* vol. 2, no. 1, pp. 56–77, 2014, doi: 10.1109/ACCESS.2014.2302442.

[5] W. Lim, S. Lee, M. Sunwoo, and K. Jo, "Hierarchical Trajectory Planning of an Autonomous Car Based on the Integration of a Sampling and an Optimization Method," *IEEE Trans. Intell. Transp. Syst.*, vol. 19, no. 2, pp. 613–626, 2018, doi: 10.1109/tits.2017.2756099.

[6] Haokan. [Online]. Available: https://haokan.baidu.com/v?pd=wisenatural&vid=10613423604342069617.

[7] J. Higgins and N. Bezzo, "Negotiating Visibility for Safe Autonomous Navigation in Occluding and Uncertain Environments," *IEEE Robot. Autom. Lett.*, vol. 6, no. 3, pp. 4409–4416, July 2021, doi: 10.1109/LRA.2021.3068701.

[8] M. Nieuwenhuisen and S. Behnke, "Search-based 3D Planning and Trajectory Optimization for Safe Micro Aerial Vehicle Flight Under Sensor Visibility Constraints," in *IEEE International Conference on Robotics and Automation (ICRA)*, 2019, doi: 10.1109/ICRA.2019.8794086.

[9] P.F. Orzechowski, A. Meyer, and M. Lauer, "Tackling Occlusions & Limited Sensor Range with Set-based Safety Verification," in *2018 21st International Conference on Intelligent Transportation Systems (ITSC)*, 2018, doi: 10.1109/ITSC.2018.8569332.

[10] M.Y. Yu, R. Vasudevan, and M. Johnson-Roberson, "Occlusion-Aware Risk Assessment for Autonomous Driving in Urban Environments," *IEEE Robot. Autom. Lett.*, vol. 4, no. 2, pp. 2235–2241, April 2019, doi: 10.1109/LRA.2019.2900453.

[11] C. Hubmann, N. Quetschlich, J. Schulz, J. Bernhard, and C. Stiller, "A POMDP Maneuver Planner For Occlusions in Urban Scenarios," in *Intelligent Vehicles Symposium*, 2019, doi: 10.1109/IVS.2019.8814179.

[12] C. Katrakazas, M. Quddus, and W.H. Chen, "A new integrated collision risk assessment methodology for autonomous vehicles," *Accid. Anal. Prev.,* vol. 127, pp. 61–79, 2019, doi: 10.1016/j.aap.2019.01.029.

[13] X. Sun *et al.*, "NFTSM control of direct yaw moment for autonomous electric vehicles with consideration of tire nonlinear mechanical properties," *Bull. Pol. Acad. Sci. Tech. Sci.*, vol. 69, no. 3, p. 137065, 2021, doi: 10.24425/bpasts.2021.137065.

[14] T. Zhao, E. Yurtsever, J.A. Paulson, and G. Rizzoni, "Formal certification methods for automated vehicle safety assessment," *IEEE Trans. Intell. Veh.,* vol. 8, no. 1, pp. 232–249, 2022, doi: 10.1109/TIV.2022.3170517.

[15] D. Wang, W. Fu, Q. Song, and J. Zhou, "Potential risk assessment for safe driving of autonomous vehicles under occluded vision," *Sci Rep.,* vol. 12, no. 1, p. 4981, 2022, doi: 10.1038/s41598-022-08810-z.

[16] L. Wang, C.F. Lopez, and C. Stiller, "Generating efficient behaviour with predictive visibility risk for scenarios with occlusions," in *2020 IEEE 23rd International Conference on Intelligent Transportation Systems (ITSC)*, 2020: IEEE, pp. 1–7, doi: 10.1109/ITSC45102.2020.9294403.

[17] H. Andersen *et al.*, "Trajectory optimization for autonomous overtaking with visibility maximization," in *2017 IEEE 20th International Conference on Intelligent Transportation Systems (ITSC)*, 2017: IEEE, pp. 1–8, doi: 10.1109/ITSC.2017.8317853.

[18] M. Koç, E. Yurtsever, K. Redmill, and Ü. Özgüner, "Pedestrian emergence estimation and occlusion-aware risk assessment for urban autonomous driving," in *2021 IEEE International Intelli-*

gent Transportation Systems Conference (ITSC), 2021: IEEE, pp. 292–297, doi: 10.1109/ITSC48978.2021.9565071.

[19] W.M.D. Chia, S.L. Keoh, C. Goh and C. Johnson, "Risk Assessment Methodologies for Autonomous Driving: A Survey," *IEEE Trans. Intell. Transp. Syst*., vol. 23, no. 10, pp. 16923–16939, Oct. 2022, doi: 10.1109/TITS.2022.3163747.

[20] J. Wang, J. Wu, and Y. Li, "The driving safety field based on driver–vehicle–road interactions," *IEEE Trans. Intell. Transp. Syst.*, vol. 16, no. 4, pp. 2203–2214, 2015, doi: 10.1109/TITS.2015.2401837.

[21] S. Hoermann, F. Kunz, D. Nuss, S. Renter, and K. Dietmayer, "Entering crossroads with blind corners. A safe strategy for autonomous vehicles," in *2017 IEEE Intelligent Vehicles Symposium (IV)*, 2017, pp. 727–732, doi: 10.1109/IVS.2017.7995803.

[22] B. Li, Y. Zhang, Y. Feng, Y. Zhang, Y. Ge, and Z. Shao, "Balancing computation speed and quality: A decentralized motion planning method for cooperative lane changes of connected and automated vehicles," *IEEE Trans. Intell. Veh.,* vol. 3, no. 3, pp. 340–350, 2018, doi: 10.1109/TIV.2018.2843159.

[23] L. Ma, J. Xue, K. Kawabata, J. Zhu, C. Ma, and N. Zheng, "Efficient sampling-based motion planning for on-road autonomous driving," *IEEE Trans. Intell. Transp. Syst.,* vol. 16, no. 4, pp. 1961–1976, 2015, doi: 10.1109/TITS.2015.2389215.

[24] T. Shimizu and P. Raksincharoensak, "Motion planning via optimization of risk quantified by collision velocity accompanied with AEB activation," in *2017 IEEE International Conference on Vehicular Electronics and Safety (ICVES)*, 2017: IEEE, pp. 19–25, doi: 10.1109/ICVES.2017.7991895.

[25] The European New Car Assessment Programme. [Online]. Available: https://www.euroncap.com/

[26] Jianqiang Wang, Jian Wu, Xunjia Zheng, Daiheng Ni, Keqiang Li, "Driving safety field theory modeling and its application in pre-collision warning system," *Transp. Res. Part. C-Emerg. Technol.*, vol. 72, no. 4, pp. 306–324, 2016, doi: 10.1016/j.trc.2016.10.003.

[27] Z. Huang *et al*., "Path planning and cooperative control for automated vehicle platoon using hybrid automata," *IEEE Trans. Intell. Transp. Syst*., vol. 20, no. 3, pp. 959–974, 2018, doi: 10.1109/TITS.2018.2841967.

[28] F. Pan *et al*., "Lane-changing risk analysis in undersea tunnels based on fuzzy inference," *IEEE Access*, vol. 8, pp. 19512–19520, 2020, doi: 10.1109/ACCESS.2020.2968584.

[29] J. Ding, R. Dang, J. Wang, and K. Li, "Driver intention recognition method based on comprehensive lane-change environment assessment," in *Intelligent Vehicles Symposium Proceedings*, 2014, pp. 214–220, doi: 10.1109/IVS.2014.6856483.

[30] Y. Qian, H. Sun, and S. Feng. "Obstacle avoidance method of autonomous vehicle based on fusion improved A*APF algorithm," *Bull. Pol. Acad. Sci. Tech. Sci*., vol. 71, no. 2, p. e144624, 2023, doi: 10.24425/bpasts.2023.144624.